Oxygen semi-permeation properties of La 1– x Sr x FeO 3–δ perovskite membranes under high oxygen gradient

Eva Deronzier, Thierry Chartier, Pierre-Marie Geffroy

Oxygen semi-permeation properties of $La_{1-x}Sr_xFeO_{3-\delta}$ perovskite membranes under high oxygen gradient

E. Deronzier[a], T. Chartier [a], P.-M. Geffroy [a]

[a] IRCER, CNRS, Université de Limoges, *CEC, 12 Rue Atlantis, 87068 Limoges, France*

Abstract

This work is focused on the evaluation of oxygen semi-permeation performances under high oxygen gradient of free cobalt perovskite membrane materials, $La_{1-x}Sr_xFeO_{3-\delta}$ perovskite. The best electrochemical performances were obtained for $La_{0.3}Sr_{0.7}FeO_{3-\delta}$ perovskite membrane with oxygen fluxes of 1.7 10^{-3} $mol.m^{-2}.s^{-1}$ at 900°C. For a better understanding of oxygen transport through $La_{1-x}Sr_xFeO_{3-\delta}$ perovskite membranes, the oxygen diffusion, oxygen incorporation and desorption coefficients were determined under high oxygen gradient in relation to the temperature for $La_{1-x}Sr_xFeO_{3-\delta}$ (with x = 0.1, 0.3, 0.5, and 0.7) by a specific method based on oxygen semi-permeation **(FIG. 6a)**. The values of these coefficients are discussed and compared with the data reported in the literature.

Keywords: LSF perovskite, oxygen diffusion, oxygen desorption coefficient.

1. Introduction

Currently, pure oxygen is industrially produced by cryogenic process. However, this process involves a high energy consumption for the separation and the production of oxygen. In order to develop a more economical process, research has focused, for several decades, on

the development of oxygen transport membranes for the pure oxygen production. The technology of oxygen transport membrane is based on the oxygen semi-permeation phenomenon, which occurs through the ceramic membrane at high temperature and under oxygen gradient between the both faces of the membrane. However, the membrane materials must have high ionic and electronic conductivities, which is usually called mixed ionic and electronic conductors (MIEC). Electrochemical and mechanical performances of numerous MIEC have also been studied during this last decade. Among these materials, $Ba_{0.5}Sr_{0.5}Co_{0.8}Fe_{0.2}O_{3-\delta}$ (BSCF) [1 2 3 4] and $La_{1-x}Sr_XCo_{1-y}Fe_yO_{3-\delta}$ (LSCF) [5 6 7 8] are promising membrane materials and have been widely cited in the literature. However, these materials contain cobalt, which is toxic and can precipitate during sintering at high temperature. Indeed, the surface of BSCF and LSCF samples sintered at 1150°C shows a secondary phase exclusively located at grain boundary at the sample surface, which decreases the ionic and electronic conductivities of the membrane material [9]. Thus, the research is currently interesting in the development of more stable materials without cobalt, containing lanthanum and iron by substituting Fe with a judicious cation in the B site like Al [10], Cr [11], Ga [12 13], Ta [14], Ti [15 16]. For instance, the oxygen flux is about 0.12 10^{-2} ml.cm^{-2}.min^{-1} (8.5 10^{-4} mol.m^{-2}.s^{-1}) at 900°C through a 1 mm thick $La_{0.5}Sr_{0.5}Fe_{0.7}Ga_{0.3}O_{3-\delta}$ dense membrane under an air/Ar gradient [17]. Park et al. [15] have reported a similar oxygen flux of 0.11 10^{-2} ml.cm^{-2}.min^{-1} (8 10^{-4} mol.m^{-2}.s^{-1}) at 900°C with a $La_{0.6}Sr_{0.4}Fe_{0.8}Ti_{0.2}O_{3-\delta}$ dense membrane under an air/He gradient. Gurauskis et al. [14] have reported a very high oxygen flux of 4.2 ml.cm^{-2}.min^{-1} (3.1 10^{-2} mol.m^{-2}.s^{-1}) at 900°C for a very thin (20 µm) dense $La_{0.2}Sr_{0.8}Fe_{0.8}Ta_{0.2}O_{3-\delta}$ membrane under an air/Ar-O_2-H_2 gradient. However, $La_{1-x}Sr_xFeO_{3-\delta}$ materials (LSF) have suitable mechanical properties and high electronic and ionic conductivities then, can therefore be used as dense membrane. Electronic and ionic conduction properties of LSF materials have been extensively reported, for instance in the following references [18 19 20 21]. Bucher et al. [18] have reported an

electronic conductivity of 60 $S.cm^{-1}$ at 900°C for $La_{0.4}Sr_{0.6}Fe0_{3-\delta}$ material under an oxygen partial pressure of 0.21 atm. The electronic conductivity decreases with decreasing oxygen partial pressure and increasing temperature above 400°C. The electronic conductivity also decreases significantly with increasing concentration of oxygen vacancies (i.e. with increasing strontium content in the material composition). Patrakeev et al. [19] have reported an ionic conductivity of 0.366 $S.cm^{-1}$ at 900°C for $La_{0.5}Sr_{0.5}FeO_{3-\delta}$ material. This conductivity increases with the strontium content until x = 0.5, then decreases when x > 0.5. Some studies reported the oxygen semi-permeation properties of $La_{1-x}Sr_xFeO_{3-\delta}$ materials (LSF) [22 23 24]. Although the conduction properties of LSF materials have been widely published, this work aims to give a better understanding of electrochemical performances of LSF membranes. In this respect, a particular attention is given to the accurate determination of oxygen bulk diffusion and surface exchange coefficients for LSF material series, obtained via a specific semi-permeation method. The originality of this work is the determination of oxygen desorption and incorporation coefficients for $La_{1-x}Sr_xFeO_{3-\delta}$ material series.

2. Experimental part

2.1. LSF membrane samples

The LSF perovskite powders were synthesized by the citrate method and prepared from pure precursors of nitrate, i.e., $La(NO_3)_3.6H_2O$ (99.9%, Alfa Aesar), $Sr(NO_3)_2$ (99.0% min, Alfa Aesar) and $Fe(NO_3)_3.9H_2O$ (98+%, Alfa Aesar). This synthesis was detailed in a previous study [25]. After synthesis, these powders were calcined at 1100°C for 5 h to obtain the perovskite phase. The calcined perovskite powders were attrition-milled for 5 h in ethanol at 1100 rpm to obtain a suitable granulometry adapted to the tape-casting process with d_{50}= 0.6 µm. Then, the perovskite powders were treated at 700°C for 30 min to remove the eventual organic pollution caused during the attrition-milling in a nylon bowl.

The LSF perovskite membranes were manufactured by the tape-casting. The procedure to obtain the tape was published earlier [17] [12]. After solvent evaporation at room temperature, 150-µm-thick green tapes were cut into 30-mm-diameter discs. These discs were stacked and laminated at 60°C under a pressure of 50 MPa to obtain membranes with a thickness of approximately 1 mm and diameter of approximately 24 mm after sintering. The green membranes were heated at 600°C to remove organic components and then sintered in air at 1150-1350°C for 8 hours to reach a relative density higher than 95%. The optimal conditions of membrane sintering are detailed in Supplementary Material. The relative density of the sintered membrane samples was measured by Archimedes's method.

2.2. Characterization of membrane materials

X-ray diffraction analyses at room temperature were carried out on calcined powders with a D8 advance diffractometer with CuKα1. The patterns were recorded in the 10-70° 2θ range with a step of 0.02° and exposure time of 1.1 s per step.

The density of each LSF powder has been measured by helium pycnometer (AccuPyc II 1340). After sintering, the microstructures of membranes were observed using scanning electron microscopy (JEOL IT 300 LV).

The oxygen semi-permeation and oxygen electrochemical activities, on both membrane surfaces, were measured using a home made setup (FIG. 1), as described in previous studies [26] [27]. A dense membrane (1 mm thick and 24 mm diameter) was sealed between two alumina tubes with gold O-rings to obtain an air-tight system. Gas flows are adjusted by flowmeters in two chambers (synthetic air to the chamber below and argon to the chamber above, see FIG. 1), producing an oxygen partial pressure gradient through the membrane.

Oxygen semi-permeation fluxes are calculated in the temperature range of 600-1000°C from equation (1), and the oxygen partial pressure in the argon flow inlet (P_{2in}) and outlet of chamber (P_2) are measured in using YSZ-oxygen sensors.

$$J_{O2} = \frac{D_{Ar}}{V_m}\frac{(P_2 - P_{2\,in})}{S} \qquad (1)$$

J_{O2}: oxygen flux through the membrane in mol.m^{-2}.s^{-1},

D_{Ar}: argon flow in l.s^{-1} (= 3.33 10^{-3} l.s^{-1}),

V_m: molar volume of argon in l.mol^{-1} (= 24 l.mol^{-1} at 20°C under 1 atm),

S: apparent membrane surface or membrane section (= 3.14 10^{-4} m^2),

P_2: measured oxygen partial pressure in argon flux outlet of the chamber (in atmosphere),

P_{2in}: oxygen partial pressure in argon flux inlet of the chamber (≈10^{-6} atm).

In each chamber, a system of microelectrodes consisting of a gold electrode and a zirconia micro-tip electrode measures the difference of oxygen activities in the gas close to the vicinity of surface ($pO_{2\ gas}$) and at the membrane surface ($pO_{2\ surface}$), on each face of the membrane (FIG. 1). Indeed, the system of microelectrodes measures directly the difference of oxygen chemical potential at the oxygen-rich $\left(\Delta\mu^{i}_{O2\,(s)}\right)$ and oxygen-lean $\left(\Delta\mu^{d}_{O2\,(s)}\right)$ surfaces of the membrane from the following Nernst relationships (2) and (3):

$$\Delta\mu^{i}_{O2\,(s)} = 4FE_{S1} \qquad (2)$$

$$\Delta\mu^{d}_{O2\,(s)} = 4FE_{S2} \qquad (3)$$

where F is the Faraday constant, E_{S1} and E_{S2} are the electromotive forces of the microelectrode system at the oxygen-rich and at the oxygen-lean surfaces of the membrane, respectively.

It is possible to determine the gradient of the oxygen chemical potential through the bulk of the membrane $\left(\Delta\mu^{bulk}_{O2}\right)$ from the following relationship (4):

$$\Delta\mu_{O2}^{\text{bulk}} = \Delta\mu_{O2}^{total} - \Delta\mu_{O2}^{i} - \Delta\mu_{O2}^{d} = \text{RT}\ln\frac{P_2}{\text{pO}_{2\,(\text{air})}} - 4\text{F}(E_{S1} + E_{S2}) \qquad (4)$$

where R is the universal gas constant and T, the temperature (in Kelvin),

$\Delta\mu_{O2}^{\text{total}}$: the gradient of oxygen chemical potential between the two chambers or through the membrane.

$\text{pO}_{2\,(\text{air})}$: oxygen partial pressure in synthetic air flow outlet the chamber (≅ 0.21 atms.)

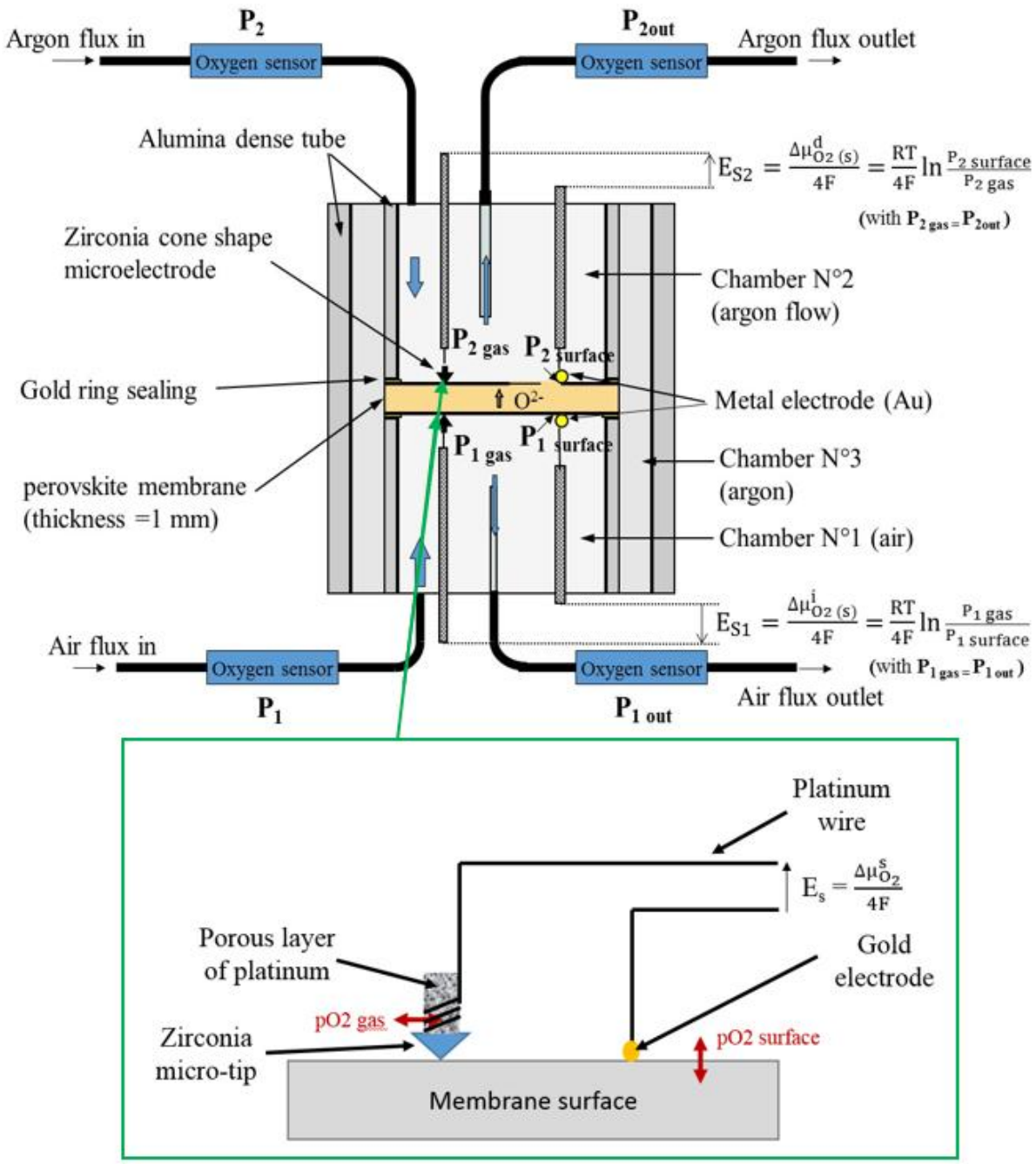

FIG. 1: Experimental setup for the measurement of oxygen fluxes and oxygen activity gradient at the membrane surfaces

3. Results and discussion

3.1. Powder characterization

FIG. 2 shows the X-ray diffraction patterns of the synthetized LSF powders. Only main pics have been indexed in FIG. 2. $La_{0.1}Sr_{0.9}FeO_{3-\delta}$ powder (LSF19) has a perovskite phase

with a cubic structure and a secondary phase with a tetragonal structure. The diffraction pattern of $La_{0.3}Sr_{0.7}FeO_{3-\delta}$ (LSF37) shows a pure perovskite phase with a cubic structure. $La_{0.5}Sr_{0.5}FeO_{3-\delta}$ (LSF55) powder has a pure perovskite phase with a rhombohedral structure, while the diffraction patterns of $La_{0.7}Sr_{0.3}FeO_{3-\delta}$ (LSF73), $La_{0.9}Sr_{0.1}FeO_{3-\delta}$ (LSF91) and $LaFeO_{3-\delta}$ (LF) powders show a perovskite phase with an orthorhombic structure without apparent secondary phase. These results are in good agreement with the literature data [23] [28] [19]. However, LSF19, LSF37 and LSF73 powders sometimes can show a mixture of two phases (a maim perovskite phase and a secondary phase). Indeed, according to Dann et al. [28], the diffraction pattern of the LSF73 powder shows the coexistence of two phases while Ten Elshof et al. [23] reported that the LSF73 powder shows a pure perovskite phase (without secondary phase).

FIG. 2: X-ray diffraction patterns of LSF powders

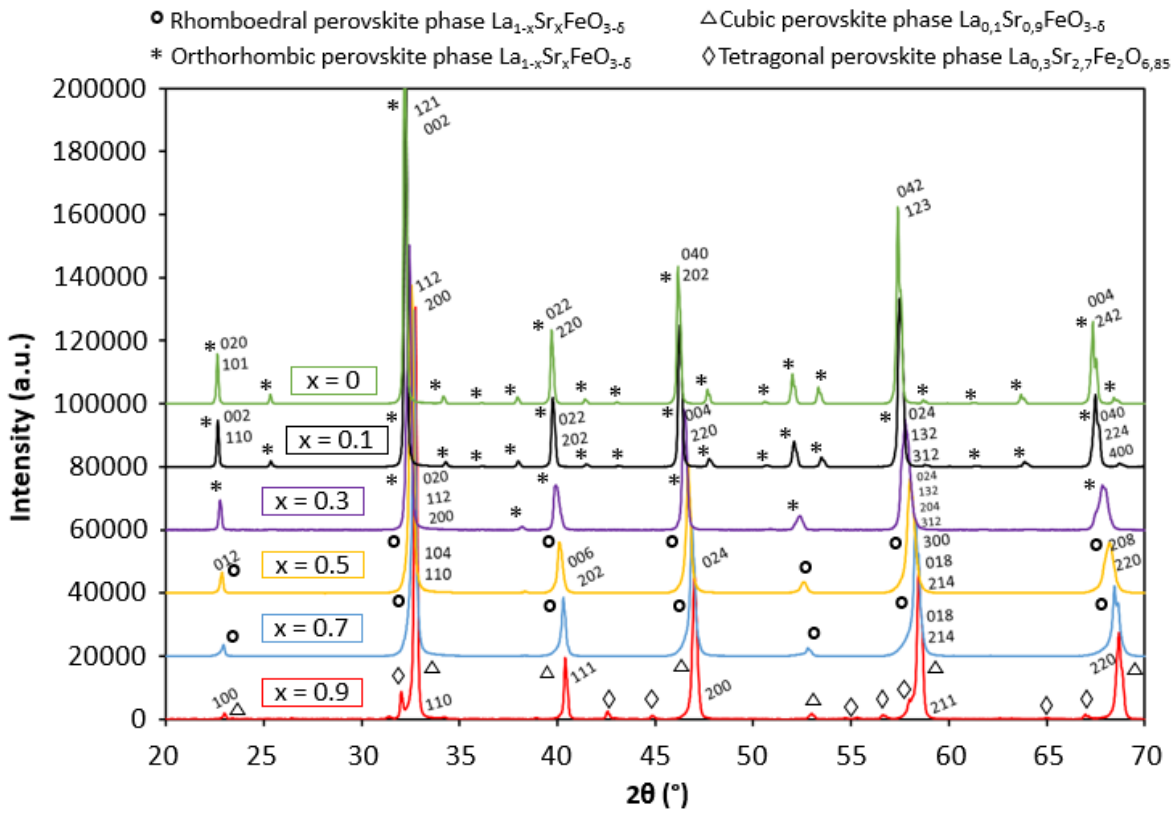

The density of each powder has been evaluated. The lower density, 5.37±0.02, is obtained for LSF19 powder and the higher, 6.46±0.02, is obtained for LF powder. The density of perovskite powders increased with La content, as expected. Densities are shown in Supplementary Material.

FIG. 3 shows the different microstructures at the surface of LSF37, LSF55, LSF73 and LSF91 membranes. Few micro-porosities were present at the membranes surface, which is in agreement with the relative density of the membrane samples. This residual porosity was likely linked to residual agglomerates that were present after the milling step [9]. TABLE 1 shows grain size for LSF membranes. There was no significant impact of strontium content on grain size of sintered membranes.

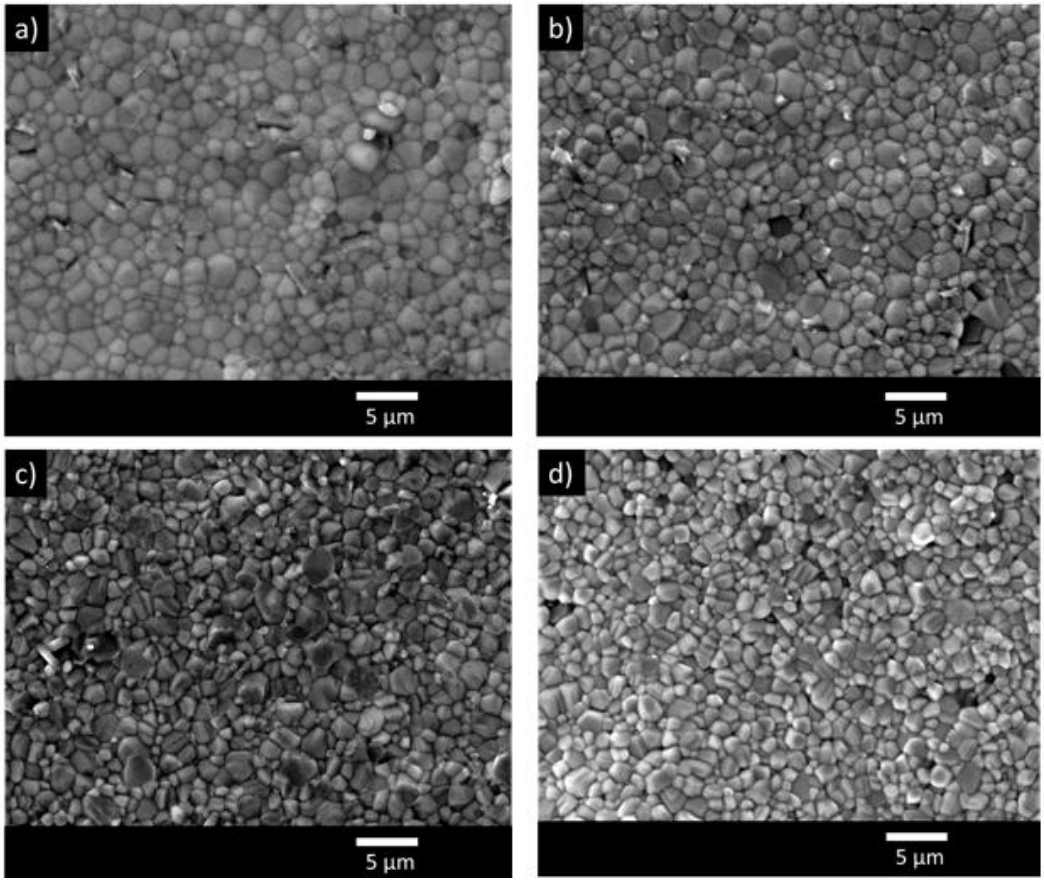

FIG. 3: Micrographies of the membrane surface obtained by SEM for a) LSF37 b) LSF55, c) LSF73, and d) LSF91 membranes

TABLE I: Grain size of LSF membranes

Composition	Grain size range (µm)
$\mathbf{La_{0,3}Sr_{0,7}FeO_{3-\delta}}$	1-3.5
$\mathbf{La_{0,5}Sr_{0,5}FeO_{3-\delta}}$	0.5-3
$\mathbf{La_{0,7}Sr_{0,3}FeO_{3-\delta}}$	0.5-3
$\mathbf{La_{0,9}Sr_{0,1}FeO_{3-\delta}}$	0.5-2.5

3.2. Oxygen semi-permeation through LSF membranes under high oxygen gradient

FIG. 4 shows the evolution of oxygen flux versus the temperature for the LSF37, LSF55, LSF73 and LSF91 membranes. Unfortunately, the mechanical cohesion of LSF19 membranes is too low for the suitable oxygen semi-permeation measurements. The highest oxygen flux

was obtained for LSF37 membrane with 1.7 10^{-3} $mol.m^{-2}.s^{-1}$ at 900°C. Kharton et al. [13] reported a similar result for a same composition of membrane material. However, the oxygen flux of our LSF55 membrane is 1.5 times lower than the flux obtained by Kharton et al. [10] (TABLE 2). In the same way, the oxygen fluxes through our LSF73 and LSF91 membranes were 3-8 times lower than the oxygen fluxes reported by Ten Elshof et al. [22] for similar compositions of membrane materials (TABLE 2). These variations of oxygen flux performances, reported in the literature for a similar material, could be linked to the oxygen semi-permeation measurement conditions (oxygen partial pressure gradient and measurement method in particular) and to the microstructure (grain size, surface polishing) of the membrane material.

For LSF samples, the oxygen flux increased with strontium content (TABLE 2) over the full temperature range of this study, as expected. These observations are in agreement with results reported by Kharton et al. [10]. However, authors reported that the fluxes obtained for a LSF55 membrane became higher than those obtained through a LSF37 membrane above 950°C. Patrakeev et al. [19] reported that, at 900°C, oxygen fluxes obtained through $La_{0.8}Sr_{0.2}FeO_{3-\delta}$ (LSF82) and LSF19 membranes were similar over the full oxygen partial pressure range used in the study. Oxygen semi-permeation fluxes through $La_{0.6}Sr_{0.4}FeO_{3-\delta}$ (LSF64) and LSF37 were similar and higher than those obtained from LSF82 and LSF91 membranes. Authors reported the highest flux for LSF55 membrane [19]. Moreover, this work shows oxygen fluxes through LSF55 membrane were 1.5 times higher than the oxygen fluxes obtained through $La_{0.5}Sr_{0.5}Fe_{0.7}Ga_{0.3}O_{3-\delta}$ (LSFGa5573) et $La_{0.6}Sr_{0.4}Fe_{0.8}Co_{0.2}O_{3-\delta}$ (LSFCo6482) with similar thickness and measurement conditions [29].

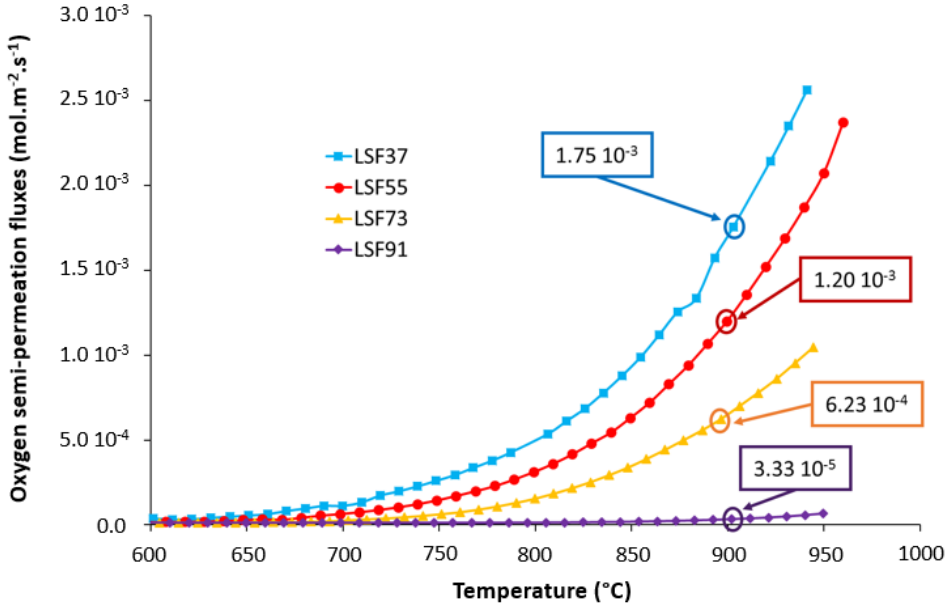

FIG. 4: Temperature dependence of the oxygen semi-permeation fluxes through dense LSF membranes under an air (100 ml.min^{-1})/argon (200 ml.min^{-1}) gradient

TABLE II: Oxygen semi-permeation fluxes for LSF, LSFGa5573 and LSFCo6482 membranes at 900°C

Material	**Reference**	**Oxygen semi-permeation flux (mol.m^{-2}.s^{-1})**
$La_{0.3}Sr_{0.7}FeO_{3-\delta}$	This work	$1.7\ 10^{-3}$
$La_{0.5}Sr_{0.5}FeO_{3-\delta}$		$1.2\ 10^{-3}$
$La_{0.7}Sr_{0.3}FeO_{3-\delta}$		$6.2\ 10^{-4}$
$La_{0.9}Sr_{0.1}FeO_{3-\delta}$		$3.3\ 10^{-5}$
$La_{0.3}Sr_{0.7}FeO_{3-\delta}$	Kharton et al. [13]	$1.9\ 10^{-3}$
$La_{0.5}Sr_{0.5}FeO_{3-\delta}$	Kharton et al. [10]	$1.8\ 10^{-3}$
$La_{0.7}Sr_{0.3}FeO_{3-\delta}$	Ten Elshof et al. [22]	$1.6\ 10^{-3}$
$La_{0.9}Sr_{0.1}FeO_{3-\delta}$		$2.5\ 10^{-4}$
$La_{0.5}Sr_{0.5}Fe_{0.7}Ga_{0.3}O_{3-\delta}$	Guironnet et al. [29] [17]	$8.5\ 10^{-4}$
$La_{0.6}Sr_{0.4}Fe_{0.8}Co_{0.2}O_{3-\delta}$		$7.3\ 10^{-4}$

As reported in our previous works [26 27], the oxygen diffusion coefficient D_O and the oxygen incorporation and oxygen desorption coefficients, k_i and k_d respectively, were evaluated from the following relationships (5), (6) and (7), respectively:

$$D_o = \frac{4RTLJ_{O_2}}{C_O \Delta\mu_{O_2}^{bulk}} \quad (5)$$

$$k_i = 2J_{O_2} \Big/ \left(C_O \left(\exp\left(\frac{(1-n)\Delta\mu_{O_2}^{i}}{RT} \right) - \exp\left(\frac{-n\Delta\mu_{O_2}^{i}}{RT} \right) \right) \right) \quad (6)$$

$$k_d = 2J_{O_2} \Big/ \left(C_O \left(\exp\left(\frac{(1-n)\Delta\mu_{O_2}^{d}}{RT} \right) - \exp\left(\frac{-n\Delta\mu_{O_2}^{d}}{RT} \right) \right) \right) \quad (7)$$

with L: membrane thickness, J_{O_2}: oxygen flux through the membrane, Co: molar oxygen concentration in the membrane close to the oxygen lean surface, $\Delta\mu_{O_2}^{bulk}$: gradient of oxygen chemical potential through the membrane bulk (FIG. 6a), $\Delta\mu_{O_2}^{i}$: gradient of oxygen chemical potential between the gas at the vicinity of the oxygen rich surface and the membrane bulk close to the oxygen rich surface (FIG. 6a), $\Delta\mu_{O_2}^{d}$: gradient of oxygen chemical potential between the gas at the vicinity of the oxygen lean surface and the membrane bulk close to the oxygen lean surface (FIG. 6a), n: exponent coefficient, constant between 0 and 1 (n = 0.5 for mixed conductors).

TABLE 3 shows the oxygen bulk diffusion coefficients D_O (or D*), oxygen incorporation coefficients k_i, and oxygen desorption coefficients k_d (or k*) obtained using the oxygen semi-permeation method (or isotopic exchange method with coefficients noted with *) for $La_{1-x}Sr_xFeO_{3-\delta}$ perovskite with and without doping. The Do and D* coefficients were similar for the LSF91 membranes. The same trend was observed for k_d and k* coefficients. However, these results were obtained from different oxygen partial pressure conditions and slight

discrepancies between D_O and D* (or k_d and k*) were mainly due to experimental conditions used by these two methods. The oxygen incorporation coefficients (k_i) are significantly higher (from 2 to 6 times) than the oxygen desorption coefficients (k_d) or k* for each material studied in this work. These results have been confirmed in other material series in previous work [26]. This means that the kinetics of oxygen incorporation reactions are very fast in comparison to the kinetics of oxygen desorption reactions, as discussed in next section (see FIG. 6).

TABLE III: Oxygen bulk diffusion and surface exchange coefficients for LSF, LSFGa5573 and LSFCo6482 membranes at 900°C

Material	**Reference**	**pO_2 at the oxygen lean chamber (atm.) or at condition measurements**	**D_O (or D*) ($cm^2.s^{-1}$)**	**k_i (or k*) ($cm.s^{-1}$) estimated at 0.065 atm. from eq. 13**	**k_d (or k*) ($cm.s^{-1}$) estimated at 0.065 atm. from eq. 13**
$La_{0.3}Sr_{0.7}FeO_{3-\delta}$	This work (semi-permeation method)	$3.5\ 10^{-3}$	$7\ (\pm2)\ 10^{-7}$	$1.0\ (\pm0.5)\ 10^{-5}$	$5\ (\pm1)\ 10^{-6}$
$La_{0.5}Sr_{0.5}FeO_{3-\delta}$		$2.5\ 10^{-3}$	$6\ (\pm2)\ 10^{-7}$	$5\ (\pm1)\ 10^{-6}$	$3\ (\pm1)\ 10^{-6}$
$La_{0.7}Sr_{0.3}FeO_{3-\delta}$		$1.3\ 10^{-3}$	$3\ (\pm1)\ 10^{-7}$	$7\ (\pm2)\ 10^{-6}$	$1.2\ (\pm0.5)\ 10^{-6}$
$La_{0.9}Sr_{0.1}FeO_{3-\delta}$		$7.2\ 10^{-5}$	$4\ (\pm1)\ 10^{-9}$	$1.0\ (\pm0.5)\ 10^{-6}$	$2\ (\pm0.5)\ 10^{-7}$
$La_{0.5}Sr_{0.5}Fe_{0.7}Ga_{0.3}O_{3-\delta}$	Guironnet et al. [29] (semi-permeation method)	$\cong 2\ 10^{-3}$	$6\ (\pm2)\ 10^{-7}$	$5\ (\pm2)\ 10^{-6}$	$2\ (\pm0.5)\ 10^{-6}$
$La_{0.6}Sr_{0.4}Fe_{0.8}Co_{0.2}O_{3-\delta}$		$\cong 2.5\ 10^{-3}$	$1.6\ (\pm0.3)\ 10^{-7}$	$8\ (\pm2)\ 10^{-6}$	$3\ (\pm1)\ 10^{-6}$
$La_{0.6}Sr_{0.4}FeO_{3-\delta}$	Ishigaki et al. [24] (isotopic exchange method)	$6.5\ 10^{-2}$	(D*) $6\ (\pm1)\ 10^{-7}$	(k*) $1.2\ (\pm0.5)\ 10^{-5}$	
$La_{0.75}Sr_{0.25}FeO_{3-\delta}$		$6.5\ 10^{-2}$	(D*) $3.4\ (\pm0.5)\ 10^{-8}$	(k*) $1.0\ (\pm0.5)\ 10^{-6}$	
$La_{0.9}Sr_{0.1}FeO_{3-\delta}$		$6.5\ 10^{-2}$	(D*) $3.2\ (\pm0.5)\ 10^{-9}$	(k*) $5\ (\pm1)\ 10^{-7}$	

The oxygen exchange coefficients obtained by oxygen isotopic exchange method are close or same order of magnitude of the coefficient of the oxygen desorption. This result can be expected because the incorporation reaction of O^{18} in the solid oxide during the isotopic exchange with the solid oxide, as reported in the reaction (8), involves the presence of oxygen vacancies (or sites to receive the O^{18} atoms from the gas) in the oxide. In other terms, the incorporation of O^{18} in the solid oxide involves a mechanism including two main steps working in series: the incorporation of one O^{18} in the solid with the consumption of one oxygen vacancy site, and the desorption of one O^{16} from the solid associated to the creation of one oxygen vacancy site, as reported in reaction (9).

$$O_{O\,(s)}^{16} + \tfrac{1}{2}O_{2\,(g)}^{18} \xrightarrow{k^*} \tfrac{1}{2}O_{2\,(g)}^{16} + O_{O\,(s)}^{18} \qquad (8)$$

$$O_{O\,(s)}^{16} + \tfrac{1}{2}O_{2\,(g)}^{18} + V_{O\,(s)}^{\bullet\bullet} \xrightarrow{k_i} O_{O\,(s)}^{16} + O_{O(s)}^{18} + 2h^{\bullet} \xrightarrow{k_d} \tfrac{1}{2}O_{2\,(g)}^{16} + O_{O\,(s)}^{18} + V_{O\,(s)}^{\bullet\bullet} \qquad (9)$$

As the oxygen isotopic exchange kinetics are governed by the slower step, in our case the oxygen desorption reactions, the k* coefficients values by isotopic exchange method are usually close to the oxygen desorption coefficients (k_d, or at the oxygen lean side) obtained by oxygen semi-permeation method, and lower than the oxygen incorporation coefficients (k_i) obtained by semi-permeation method. This clearly shows one advantage of the semi-permeation method in comparison the usual isotopic exchange, which makes it possible to dissociate the oxygen incorporation and desorption coefficients.

From a chemical point of view, reaction (9) can be dissociated to the oxygen incorporation reaction (10) with the k_i coefficient which corresponds to the forward reaction rate per unit area (called oxygen incorporation coefficient in this work). In the oxygen desorption reaction

(11), the k_d coefficient corresponds to the reverse reaction rate per unit area (called oxygen desorption coefficient in this work).

$$\frac{1}{2}O_{2\,(g)} + V_{O\,(s)}^{\bullet\bullet} \xrightarrow{k_i} O_{O(s)} + 2h^{\bullet} \qquad (10)$$

$$O_{O(s)} + 2h^{\bullet} \xrightarrow{k_d} \frac{1}{2}O_{2\,(g)} + V_{O\,(s)}^{\bullet\bullet} \qquad (11)$$

The oxygen-semi-permeation measurement, which allows to dissociate and to evaluate the incorporation and desorption coefficients k_i and k_d, is carried out with a succession of steady states at different temperatures, and not in an equilibrium state. These thermodynamic conditions lead to promote one direction of the reaction of oxygen surface exchanges between the gas and the oxide surface, in your case the incorporation reaction at the membrane surface in contact with oxygen rich side and the desorption reaction in contact with oxygen lean side.

Using the semi-permeation method, the k_d coefficients of the LSF55 membrane are similar k_d coefficient reported for LSFGa5573 and LSFCo6482 materials. Moreover, this k_d coefficient and the D_O coefficient increased significantly with the Sr content in LSF materials. These observations are in agreement with those reported by Ishigaki et al. [24] for $La_{0.9}Sr_{0.1}FeO_{3-\delta}$, $La_{0.75}Sr_{0.25}FeO_{3-\delta}$ and $La_{0.6}Sr_{0.4}FeO_{3-\delta}$ membranes.

The D_O coefficient of LSF55 sample was similar to the one obtained for LSFGa5573 membrane and was higher than the one obtained for LSFCo6482. Thus, electrochemical performances of LSF55 membrane should be likely similar than those of LSFGa5573 and LSFCo6482 membranes.

FIG. 5 shows the Arrhenius plots of oxygen semi-permeation fluxes versus 1/T (T: absolute temperature in K) for LSF membranes. The slope of the Arrhenius plot allows to evaluate the activation energy (E_a) of the mechanism limiting oxygen transport through the

membrane (TABLE 4). This rate determining step can depend on temperature. In the case of LSF materials, the Arrhenius plots show only one slope over the full temperature range used in this study (600-950°C), suggesting the same rate determining step at high and low temperature.

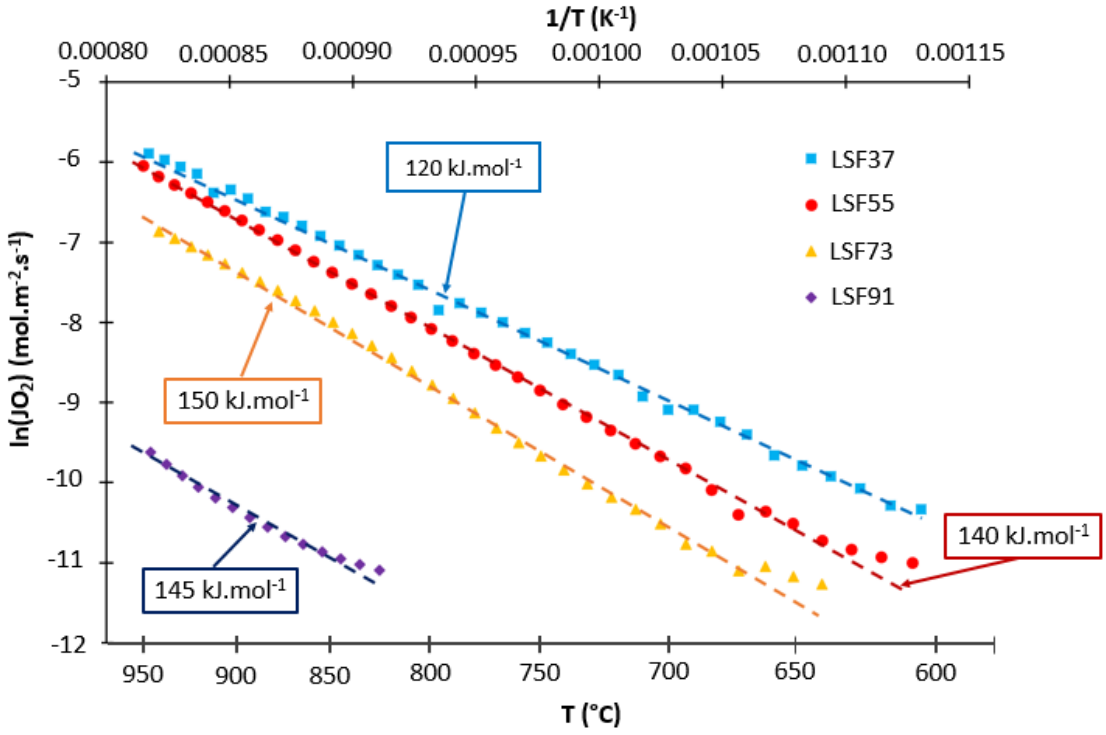

FIG. 5: Arrhenius plots of oxygen fluxes versus 1/T for LSF37, LSF55, LSF73 and LSF91 membranes

At 900°C, the profile of the oxygen chemical potential through LSF membranes reported on the FIG. 6 clearly shows a large gradient of oxygen chemical potential at the oxygen lean membrane surface, which suggests that the oxygen permeability is mainly governed by the oxygen desorption kinetics at high and low temperature, as expected.

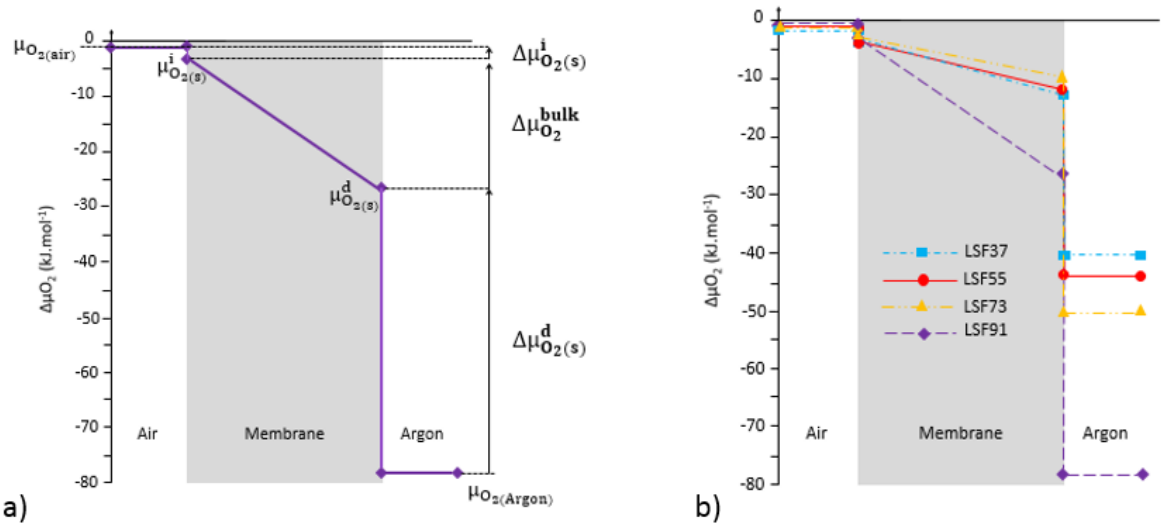

FIG. 6: a) Profile of the oxygen chemical potential through LSF91 perovskite membrane at 900°C with three main steps : oxygen incorporation, bulk diffusion, and desorption, b) Profiles of the oxygen chemical potential through LSF37, LSF55, LSF73 and LSF91 membranes at 900°C

However, Tsipis et al. [20] reported that the oxygen semi-permeation flux through LSF55 membrane is governed by both oxygen bulk diffusion and exchange kinetics. Kharton et al. [13] also reported the same observation for LSF37 membrane. The main reason of this slight discrepency is that the surface roughness, a low amount of secondary phase or chemical contamination at the surface [17] can strongly affect the kinetics of oxygen surface exchanges. Then, the rate determining step of oxygen transport through LSF membranes can be affected by the elaboration method and the surface preparation of the membrane material.

Addition of a doping element in the membrane composition can lead to a different rate determining step. For exemple, Kharton et al. [10] reported that the flux through $La_{0.5}Sr_{0.5}Fe_{0.9}Al_{0.1}O_{3-\delta}$ membrane is mainly governed by bulk diffusion (at high temperature). Tsipis et al. [20] reported the same observation for $La_{0.5}Sr_{0.5}Fe_{0.9}Ti_{0.1}O_{3-\delta}$ membrane. L. Guironnet [29] showed that the oxygen semi-permeation flux through the LSFGa5573 membrane is governed by the oxygen surface exchange at high temperature.

TABLE IV: Activation energies of the oxygen semi-permeation flux through LSF, LSFGa5573 and LSFCo6482 membranes

Material	Reference	E_a (650°C-850°C)	E_a (850°C-1050°C)
$\mathbf{La_{0.3}Sr_{0.7}FeO_{3-\delta}}$	This work	120 kJ.mol^{-1}	120 kJ.mol^{-1}
$\mathbf{La_{0.5}Sr_{0.5}FeO_{3-\delta}}$		140 kJ.mol^{-1}	140 kJ.mol^{-1}
$\mathbf{La_{0.7}Sr_{0.3}FeO_{3-\delta}}$		150 kJ.mol^{-1}	150 kJ.mol^{-1}
$\mathbf{La_{0.9}Sr_{0.1}FeO_{3-\delta}}$		-	145 kJ.mol^{-1}
$\mathbf{La_{0.6}Sr_{0.4}FeO_{3-\delta}}$	Ten Elshof et al. [22]	-	173 (±11) kJ.mol^{-1}
$\mathbf{La_{0.7}Sr_{0.3}FeO_{3-\delta}}$		-	206 (±12) kJ.mol^{-1}
$\mathbf{La_{0.8}Sr_{0.2}FeO_{3-\delta}}$		-	199 (±18) kJ.mol^{-1}
$\mathbf{La_{0.9}Sr_{0.1}FeO_{3-\delta}}$		-	178 (±7) kJ.mol^{-1}
$\mathbf{La_{0.5}Sr_{0.5}Fe_{0.7}Ga_{0.3}O_{3-\delta}}$	Guironnet et al. [29]	148 kJ.mol^{-1}	123 kJ.mol^{-1}
$\mathbf{La_{0.6}Sr_{0.4}Fe_{0.8}Co_{0.2}O_{3-\delta}}$		128 kJ.mol^{-1}	117 kJ.mol^{-1}

The activation energies were similar for these four LSF membranes and there was no significant impact of strontium content on the activation energies of oxygen transport mechanisms. These observations are in agreement with those reported by Ten Elshof et al. [22]. However, activation energies obtained in this work for LSF91, LSF73 and LSF55 were lower than those obtained by Ten Elshof et al. [22] for similar or close compositions of membrane material (TABLE 4). The activation energy obtained through LSF55 membrane was slightly higher than those of LSFGa5573 and LSFCo6482 membranes at high temperature.

The values of activation energy reported in this work and by Ten Elshof et al. [22] are likely affected by a systematic overestimation of the energy activation due to working conditions imposed by the oxygen semi-permeation method. This overestimation corresponds to an additional contribution linked to the pO_2 dependence on the kinetics of oxygen surface exchanges (in our case, mainly k_d) or on the oxygen bulk diffusion. The oxygen semi-permeation measurement under a large gradient of oxygen activity leads to a large variation of

pO_2 in the permeate chamber (oxygen lean chamber) in relation to the working conditions, then to the variation of k_i, k_d and to a lesser extent D_O.

In the case of a flux mainly governed by the oxygen desorption reactions, this overestimation of the activation energy $\Delta E_a^{(pO2)}$ can be evaluated from equation (12) as following:

$$\Delta E_a^{(pO2)} = R \ln \frac{k_{d\,(pO_{2\,(1)})}}{k_{d\,(pO_{2\,(2)})}} / (1/T_1 - 1/T_2) \quad (12)$$

$pO_{2\ (1)}$: equivalent oxygen partial pressure at the membrane surface in the oxygen lean chamber at T_1

$pO_{2\ (2)}$: equivalent oxygen partial pressure at the membrane surface in the oxygen lean chamber at T_2

$k_{d\,(pO_{2\,(1)})}$: coefficient of oxygen desorption at $pO_{2\,(1)}$ and at T_1

$k_{d\,(pO_{2\,(2)})}$: coefficient of oxygen desorption at $pO_{2\,(2)}$ and at T_2

It assumes here that the pO_2 dependence on k_d can be expressed as following:

$$k_d = k_d^\circ \, (pO_2/pO_2^\circ)^n \quad (13)$$

where k_d° is the surface exchange coefficient at the reference oxygen partial pressure, usually pO_2° = 0.21 atm., n is the power law parameter related to the electronic defect concentration in these materials, i.e. 0.4-0.5 for electron-rich mixed conductors (e.g. $La_{0.8}Sr_{0.2}MnO_{3-\delta}$, $La_{0.6}Sr_{0.4}Fe_{0.8}Co_{0.2}O_{3-\delta}$ and $La_{0.3}Sr_{0.7}CoO_{3-\delta}$ perovskites) [30 31 32].

From equation (13), the equation (12) can be simplified as following:

$$\Delta E_a^{(pO2)} = n\,R\,\ln \frac{pO2\,(1)}{pO2\,(2)} / (1/T_1 - 1/T_2) \quad (14)$$

The working conditions used by Ten Elshof et al. [22] lead to a large variation of pO_2 and then, according to eq. (14), to a significant overestimation of the activation energy, estimated to 30-70 kJ.mol^{-1} (resp. 5-30 kJ.mol^{-1} in this work). The overestimation of E_a linked to the pO_2

variation during the oxygen semi-permeation measurements is never clearly mentioned in the literature, although $\Delta E_a^{(pO2)}$ may be significant, estimated here to 5-30 kJ.mol^{-1}.

Then, the apparent discrepancy observed in the literature between the values of activation energy obtained by isotopic and oxygen semi-permeation methods could be directly attributed to the working conditions of the oxygen semi-permeation method.

4. Conclusion

The oxygen flux through LSF membranes increases with strontium content in LSF materials. Both the oxygen bulk diffusion and surface exchange coefficients increase with strontium content. The oxygen semi-permeation fluxes of LSF membranes (1 mm thick) are mainly governed by the oxygen desorption kinetics between 600 to 950°C.

The highest oxygen semi-permeation flux was obtained through LSF37 membrane with 1.7 10^{-3} mol.m^{-2}.s^{-1} at 900°C. However, the LSF37 or LSF membranes with x>0.7 show too low mechanical properties for oxygen semi-permeation measurements or for the eventual industrial applications as oxygen transport membranes.

Among materials studied in this work, the LSF55 material constitutes the better compromise between electrochemical and mechanical properties. In particular, the LSF55 membrane has a D_O coefficient close or higher than those of LSFGa5573 and LSFCo6482 membranes and a similar or slightly higher k_d coefficient. In this respect, LSF55 material could be one of promising materials for oxygen transport membranes or electrode materials in SOFC applications.

The semi-permeation method corresponds to a very efficient method to dissociate the oxygen incorporation and desorption coefficients, which is a potential advantage for the study of oxygen transport in the oxide materials in comparison to the usual isotopic exchange method. Nevertheless, the surface exchange coefficient, k*, measured by isotopic exchange is usually

very close to oxygen desorption coefficient obtained by oxygen semi-pemeation method. Indeed, the isotopic oxygen incorporation in the oxide involves a two main steps mechanism with the creation and comsumption of oxygen vacancies, corresponding to the desorption step of O^{16} and the incorporation step of O^{18}, respectivley. The kinetics of oxygen incorporation in the solid is mainly governed by the slower step, corresponding to the oxygen desorption step in the gas from the oxide.

The difference of activation energy (typically 30-70 $kJ.mol^{-1}$), reported in the literature, between the values obtained by isotopic exchange and oxygen semi-permeation methods could be directly attributed to the large gradient of oxygen activity imposed in the oxygen semi-permeation method.

5. References

1. M. Arnold, H. Wang, and A. Feldhoff: Influence of CO2 on the oxygen permeation performance and the microstructure of perovskite-type (Ba0.5Sr0.5)(Co0.8Fe0.2)O3−δ membranes. *J. Membr. Sci.* **293**(1), 44 (2007).

2. C. Buysse, A. Kovalevsky, F. Snijkers, A. Buekenhoudt, S. Mullens, J. Luyten, J. Kretzschmar, and S. Lenaerts: Development, performance and stability of sulfur-free, macrovoid-free BSCF capillaries for high temperature oxygen separation from air. *J. Membr. Sci.* **372**(1), 239 (2011).

3. T. Klande, O. Ravkina, and A. Feldhoff: Effect of microstructure on oxygen permeation of Ba0.5Sr0.5Co0.8Fe0.2O3−δ and SrCo0.8Fe0.2O3−δ membranes. *J. Eur. Ceram. Soc.* **33**(6), 1129 (2013).

4. A. Berenov, A. Atkinson, J. Kilner, M. Ananyev, V. Eremin, N. Porotnikova, A. Farlenkov, E. Kurumchin, H. J. M. Bouwmeester, E. Bucher, and W. Sitte: Oxygen tracer diffusion and surface exchange kinetics in Ba0.5Sr0.5Co0.8Fe0.2O3−δ. *Solid State Ion.* **268**, 102 (2014).

5. M. Katsuki, S. Wang, M. Dokiya, and T. Hashimoto: High temperature properties of La0.6Sr0.4Co0.8Fe0.2O3−δ oxygen nonstoichiometry and chemical diffusion constant. *Solid State Ion.* **156**(3), 453 (2003).

6. T. Li, T. Kamhangdatepon, B. Wang, U. W. Hartley, and K. Li: New bio-inspired design for high-performance and highly robust La0.6Sr0.4Co0.2Fe0.8O3-δ membranes for oxygen permeation. *J. Membr. Sci.* **578**, 203 (2019).

7. J. Gao, Y. Lun, N. Han, X. Tan, C. Fan, and S. Liu: Influence of nitric oxide on the oxygen permeation behavior of La0.6Sr0.4Co0.2Fe0.8O3−δ perovskite membranes. *Sep. Purif. Technol.* **210**, 900 (2019).

8. S. P. Jiang: Development of lanthanum strontium cobalt ferrite perovskite electrodes of solid oxide fuel cells – A review. *Int. J. Hydrog. Energy* **44**(14), 7448 (2019).

9. S. Baumann, F. Schulze-Küppers, S. Roitsch, M. Betz, M. Zwick, E. M. Pfaff, W. A. Meulenberg, J. Mayer, and D. Stöver: Influence of sintering conditions on microstructure and oxygen permeation of Ba0.5Sr0.5Co0.8Fe0.2O3−δ (BSCF) oxygen transport membranes. *J. Membr. Sci.* **359**(1), 102 (2010).

10. V. V. Kharton, J. C. Waerenborgh, A. P. Viskup, S. O. Yakovlev, M. V. Patrakeev, P. Gaczyński, I. P. Marozau, A. A. Yaremchenko, A. L. Shaula, and V. V. Samakhval: Mixed conductivity and Mössbauer spectra of (La0.5Sr0.5)1−xFe1−yAlyO3−δ (x=0–0.05, y=0–0.30). *J. Solid State Chem.* **179**(4), 1273 (2006).

11. M. F. Lü, E. V. Tsipis, J. C. Waerenborgh, A. A. Yaremchenko, V. A. Kolotygin, S. Bredikhin, and V. V. Kharton: Thermomechanical, transport and anodic properties of perovskite-type (La0.75Sr0.25)0.95Cr1−xFexO3−δ. *J. Power Sources* **206**, 59 (2012).

12. P. M. Geffroy, M. Reichmann, L. Kilmann, J. Jouin, N. Richet, and T. Chartier: Identification of the rate-determining step in oxygen transport through La(1−x)SrxFe(1−y)GayO3−δ perovskite membranes. *J. Membr. Sci.* **476**(Supplement C), 340 (2015).

13. V. V. Kharton, A. L. Shaulo, A. P. Viskup, M. Avdeev, A. A. Yaremchenko, M. V. Patrakeev, A. I. Kurbakov, E. N. Naumovich, and F. M. B. Marques: Perovskite-like system

(Sr,La)(Fe,Ga)O3−δ: structure and ionic transport under oxidizing conditions. *Solid State Ion.* **150**(3), 229 (2002).

14. J. Gurauskis, Ø. F. Lohne, D. S. Lagergren, E. T. Wefring, and K. Wiik: Oxygen permeation in symmetric and asymmetric La0.2Sr0.8Fe0.8Ta0.2O3−δ membranes. *J. Eur. Ceram. Soc.* **36**(6), 1427 (2016).

15. J. H. Park, K. Y. Kim, and S. D. Park: Oxygen permeation and stability of La0.6Sr0.4TixFe1−xO3−δ (x = 0.2 and 0.3) membrane. *Desalination* **245**(1), 559 (2009).

16. B. Kayaalp, S. Lee, K. Klauke, J. Seo, L. Nodari, A. Kornowski, W. Jung, and S. Mascotto: Template-free mesoporous La0.3Sr0.7Ti1-xFexO3±δ for CH4 and CO oxidation catalysis. *Appl. Catal. B Environ.* **245**, 536 (2019).

17. L. Guironnet, P.-M. Geffroy, N. Tessier-Doyen, A. Boulle, N. Richet, and T. Chartier: The surface roughness effect on electrochemical properties of La0.5Sr0.5Fe0.7Ga0.3O3-δ perovskite for oxygen transport membranes. *J. Membr. Sci.* **588**, 117199 (2019).

18. E. Bucher and W. Sitte: Defect chemical analysis of the electronic conductivity of strontium-substituted lanthanum ferrite. *Solid State Ion.* **173**(1), 23 (2004).

19. M. V. Patrakeev, J. A. Bahteeva, E. B. Mitberg, I. A. Leonidov, V. L. Kozhevnikov, and K. R. Poeppelmeier: Electron/hole and ion transport in La1−xSrxFeO3−δ. *J. Solid State Chem.* **172**(1), 219 (2003).

20. E. V. Tsipis, M. V. Patrakeev, V. V. Kharton, A. A. Yaremchenko, G. C. Mather, A. L. Shaula, I. A. Leonidov, V. L. Kozhevnikov, and J. R. Frade: Transport properties and thermal expansion of Ti-substituted La1−xSrxFeO3−δ (x=0.5–0.7). *Solid State Sci.* **7**(4), 355 (2005).

21. M. Søgaard, P. Vang Hendriksen, and M. Mogensen: Oxygen nonstoichiometry and transport properties of strontium substituted lanthanum ferrite. *J. Solid State Chem.* **180**(4), 1489 (2007).

22. J. E. ten Elshof, H. J. M. Bouwmeester, and H. Verweij: Oxygen transport through La1−xSrxFeO3−δ membranes. I. Permeation in air/He gradients. *Solid State Ion.* **81**(1), 97 (1995).

23. J. E. ten Elshof, H. J. M. Bouwmeester, and H. Verweij: Oxygen transport through La1 − xSrxFeO3 − δ membranes II. Permeation in air/CO, CO2 gradients. *Solid State Ion.* **89**(1), 81 (1996).

24. T. Ishigaki, S. Yamauchi, K. Kishio, J. Mizusaki, and K. Fueki: Diffusion of oxide ion vacancies in perovskite-type oxides. *J. Solid State Chem.* **73**(1), 179 (1988).

25. L. Guironnet, P.-M. Geffroy, F. Jouay, C. Pagnoux, N. Richet, and T. Chartier: La0.6Sr0.4Fe0.8Co0.2O3-δ electrophoretic coating for oxygen transport membranes. *Chem. Eng. Sci. X* **1**, 100008 (2019).

26. P.-M. Geffroy, E. Blond, N. Richet, and T. Chartier: Understanding and identifying the oxygen transport mechanisms through a mixed-conductor membrane. *Chem. Eng. Sci.* **162**(Supplement C), 245 (2017).

27. M. Reichmann, P.-M. Geffroy, J. Fouletier, N. Richet, and T. Chartier: Effect of cation substitution in the A site on the oxygen semi-permeation flux in La0.5A0.5Fe0.7Ga0.3O3−δ and La0.5A0.5Fe0.7Co0.3O3−δ dense perovskite membranes with A = Ca, Sr and Ba (part I). *J. Power Sources* **261**(Supplement C), 175 (2014).

28. S. E. Dann, D. B. Currie, M. T. Weller, M. F. Thomas, and A. D. Al-Rawwas: The Effect of Oxygen Stoichiometry on Phase Relations and Structure in the System La1-xSrxFeO3-δ (0 ≤ x ≤ 1, 0 ≤ δ ≤ 0.5). *J. Solid State Chem.* **109**(1), 134 (1994).

29. L. Guironnet: Compréhension de l'influence Des Paramètres Micro et Nano Structuraux Sur Les Performances Électrochimiques de Conducteurs Mixtes, Thèse de doctorat, Limoges, 2017.

30. R. A. De Souza: A universal empirical expression for the isotope surface exchange coefficients (k*) of acceptor-doped perovskite and fluorite oxides. *Phys. Chem. Chem. Phys. PCCP* **8**(7), 890 (2006).

31. RenéH. E. van Doorn, I. C. Fullarton, R. A. de Souza, J. A. Kilner, H. J. M. Bouwmeester, and A. J. Burggraaf: Surface oxygen exchange of La0.3Sr0.7CoO3 − δ. *Solid State Ion.* **96**(1), 1 (1997).

32. R. A. De Souza, J. A. Kilner, and J. F. Walker: A SIMS study of oxygen tracer diffusion and surface exchange in La0.8Sr0.2MnO3+δ. *Mater. Lett.* **43**(1), 43 (2000).

Figure Captions

Table Captions